# Infrared emission of a freestanding plasmonic membrane

Hosein Monshat,[1] Longju Liu,[2] John McClelland,[3] Rana Biswas,[2,4] and Meng Lu[1,2,a)]
[1]Department of Mechanical Engineering, Iowa State University, Ames, Iowa 50011, USA
[2]Department of Electrical and Computer Engineering, Iowa State University, Ames, Iowa 50011, USA
[3]MTEC Photoacoustics Inc., 3507 Oakland Street, Ames, Iowa 50014, USA
[4]Ames Laboratory-USDOE, Ames, Iowa 50011, USA

(Received 25 November 2017; accepted 2 January 2018; published online 16 January 2018)

This paper reports a free-standing plasmonic membrane as a thermal emitter in the near- and mid-infrared regions. The plasmonic membrane consists of an ultrathin gold film perforated with a two-dimensional array of holes. The device was fabricated using an imprint and transfer process and fixed on a low-emissivity metal grid. The thermal radiation characteristics of the plasmonic membrane can be engineered by controlling the array period and the thickness of the gold membrane. Plasmonic membranes with two different periods were designed using electromagnetic simulation and then characterized for their transmission and infrared radiation properties. The free-standing membranes exhibit extraordinary optical transmissions with the resonant transmission coefficient as high as 76.8%. After integration with a customized heater, the membranes demonstrate narrow-band thermal emission in the wavelength range of 2.5 $\mu$m to 5.5 $\mu$m. The emission signatures, including peak emission wavelength and bandwidth, are associated with the membrane geometry. The ultrathin membrane infrared emitter can be adopted in applications, such as chemical analysis and thermal imaging. *Published by AIP Publishing*. https://doi.org/10.1063/1.5017194

Designing the spectral features of metamaterials has been a strong driving force to motivating much recent research in the field of nanophotonics. In particular, metal micro- and nano-structures support surface plasmon resonances (SPRs) as a result of the collective oscillation of surface charges at metal-dielectric interfaces.[1] Surface plasmon resonances have been utilized to enable a number of new optical phenomena, such as extraordinary optical transmission (EOT), strong optical absorption, and enhanced local electromagnetic fields. These phenomena have been exploited in many applications, such as chemical and biological sensors, plasmon-enhanced photodetectors, and on-chip optical components.[2–5] Of particular interest is the interaction of plasmonics and thermal radiation. The plasmon-enhanced photothermal effect has been utilized in photothermal therapy, solar water heating, and biomolecule detection.[6–9] The SPR can also be utilized to generate a selective thermal radiation in the infrared (IR) region.[10–14]

Conventional thermal emitters are broadband with emission spectra determined by the emissivity of the material of the heated element. Recent advances in nanophotonics enable the control of optical density of states and thus achieve the selective IR radiation. For instance, photonic crystal structures have been utilized to inhibit unwanted thermal emission.[15–18] In contrast, plasmonic structures can enhance thermal emission near the SPRs.[13,19] Previous plasmonic devices utilized sub-wavelength metal structures fabricated on substrates, in which the substrate had no active role, and contributed a large thermal mass, with significant cooling and heating ramp-up times.[20,21] In addition to the fundamental air-metal SPR resonance at a wavelength ($\lambda_r$), the use of substrates creates a secondary metal-substrate SPR peak at a wavelength $n_{sub}\lambda_t$, where $n_{sub}$ is the refractive index of the substrate. Multiple resonances may exist owing to the coupling of the two SPR modes. The use of a substrate thus creates unwanted complex spectral features in the absorption and thermal emission.

Here, we demonstrate free-standing nano-hole arrays without substrates for tailoring thermal radiation. The advantages of free-standing nano-hole membranes include the single emission peak without the multiple spectral features induced by the substrate and the ability of rapid heating and cooling, which is desirable in sensing applications. This paper reports the design, fabrication, and characterization of the free-standing gold film patterned with a two-dimensional (2D) array of subwavelength holes.

As illustrated in Fig. 1(a), the membrane consists of a 2D array of holes in the ultrathin gold (Au) film. The geometry of the device, including its period ($\Lambda$), hole diameter ($d$), and membrane thickness ($t_{Au}$), can be designed to manifest plasmon resonances in a desired wavelength range. An imprint and transfer process has been developed to fabricate the free-standing membrane device.[22] The imprint step used a Poly(dimethylsiloxane) (PDMS) featuring the negative image of the 2D array pattern as the imprint mold. The pattern on the PDMS mold was imprinted to a thin film of Poly(vinyl formal) copolymer (Vinylec, Sigma-Aldrich) by pressing the mold against the copolymer dip-coated on a glass. The copolymer film was released to the water surface and subsequently picked up using a nickel frame. The transferred copolymer film was fixed on the grid and became suspended inside each 180 $\mu$m × 180 $\mu$m aperture as shown in Fig. 1(b). After the copolymer film was dried, the top surface was coated with gold using a sputter (Desktop IV, Denton Vacuum LLC). Then, the device was immersed in dichloromethane solution to remove the copolymer layer. The scanning electron microscopy (SEM) images in Figs. 1(c) and 1(d) show the fabricated free-standing membranes with $\Lambda = 2.5$ $\mu$m and 4.0 $\mu$m and hole diameters of $d = 1.2$ $\mu$m and 2 $\mu$m, respectively.

a)Author to whom correspondence should be addressed: menglu@iastate.edu

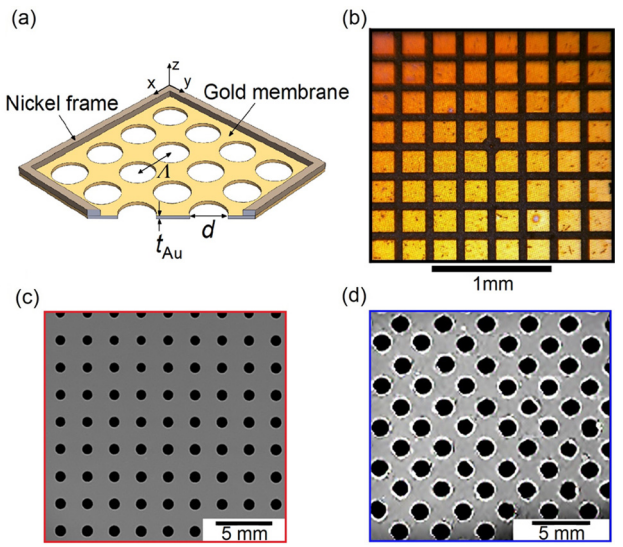


FIG. 1. (a) Schematic diagram of the free-standing Au-membrane suspended on a nickel frame (not to scale). (b) Transmitted light micrograph of the fabricated Au-membrane device with $\Lambda = 2.5\,\mu$m. The dark lines represent the nickel frame. (c) and (d) SEM images of the Au-membrane devices with the periods of $\Lambda = 2.5\,\mu$m and $\Lambda = 4.0\,\mu$m, respectively.

Metal thin films with subwavelength periodic structures can support surface plasmon-polariton (SPP) Bloch waves (BW).[23] The resonant wavelength of a SPP-mode can be estimated using the Bragg coupling equation, $\frac{2\pi}{\lambda_r}\sqrt{\frac{\varepsilon_m\varepsilon_d}{\varepsilon_m+\varepsilon_d}} = |\mathbf{k}_{||} + p\mathbf{G}_x + q\mathbf{G}_y|$, where $\omega$ and $c$ are the angular frequency and speed of light in free-space, respectively, $\varepsilon_m$ and $\varepsilon_d$ are the relative permittivity of the metal and the surrounding medium, respectively, $\boldsymbol{k}_{||}$ is the in-plane wave vector of incident light, $\boldsymbol{G}_x$ and $\boldsymbol{G}_y$ are the reciprocal vectors ($|\boldsymbol{G}_x| = |\boldsymbol{G}_y| = 2\pi/\Lambda = |\boldsymbol{G}|$), and integer index pairs ($p$, $q$) specify the order of SPP-BW modes. This work investigates the mid-IR emission perpendicular to the membrane surface when $\boldsymbol{k}_{||} = 0$ with the SPP resonance coupled to the radiative mode by the 1st order Bragg diffraction with ($p$, $q$) = (1, 0) or (0, 1) in the square lattice. To ensure that the plasmon resonance appears in the desired mid-IR wavelength range of 2 $\mu$m to 6 $\mu$m, we used a finite difference time domain (FDTD) simulation tool (FDTD Solution, Lumerical Inc.) to design the membrane structure numerically. The simulation domain was set to one-unit volume of the periodic membrane structure with the periodic boundary conditions imposed along the $x$ and $y$ directions defined in Fig. 1(a). Perfectly matched layer boundary conditions were utilized to truncate the simulation region along the $z$-direction to absorb outgoing radiations. The refractive index of Au used in the simulation was based on published data.[24] The Au membrane structure was illuminated with a normally incident, unit magnitude plane wave propagating in the $z$-axis with an electric field polarization along the $y$-axis. Both polarizations degenerate at normal incidence.

Figure 2 shows the simulation results of the Au membranes with different grating periods and membrane thicknesses. The reflection, transmission, and absorption spectra are shown in Figs. 2(a) and 2(b) for the membranes with two different grating periods. The plasmonic resonance wavelengths locate at $\lambda_r = 2.85\,\mu$m and 4.45 $\mu$m for the device with $\Lambda = 2.5\,\mu$m and 4.0 $\mu$m, respectively. Figure 2(b) shows the well-known Wood's anomaly associated with the 1st order (1, 0) or (0, 1) SPP mode at which the transmission vanishes

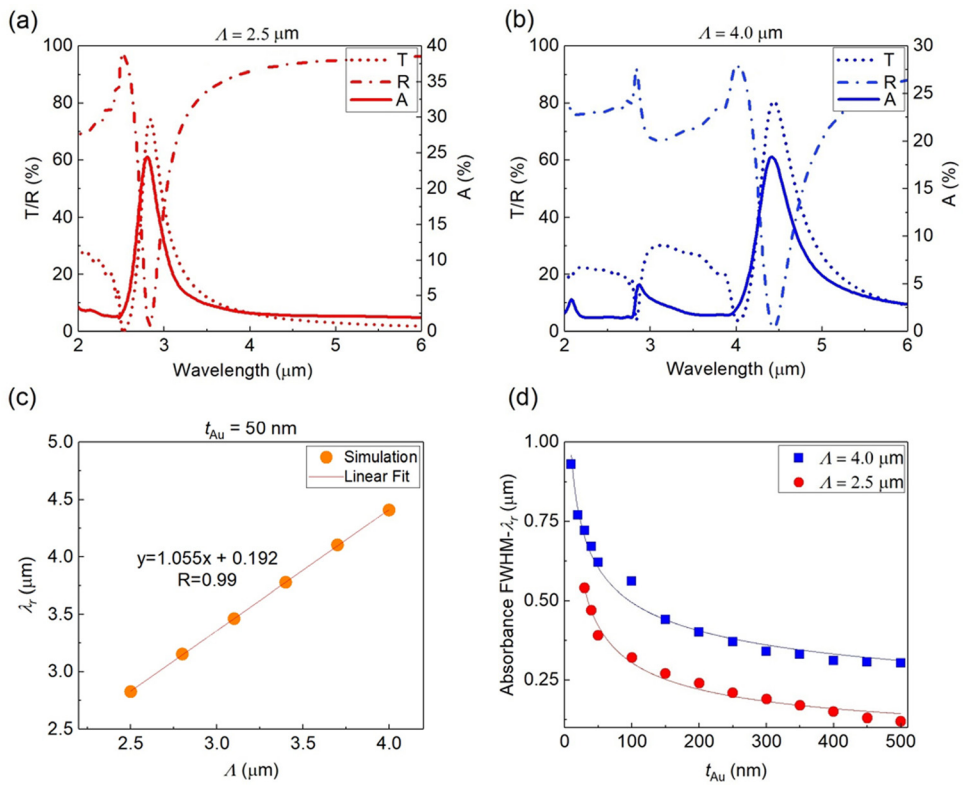


FIG. 2. Electromagnetic simulation of the reflection, transmission, and absorption characteristics of the membrane devices. (a) and (b) Reflectance, transmittance, and absorbance of the device with periods of $\Lambda = 2.5\,\mu$m and $\Lambda = 4.0\,\mu$m, respectively. The membrane thickness of both samples is $t_{Au} = 50$ nm. (c) The linear relation between the resonance wavelength and the array period. (d) The change of FWHM of the sample absorbance as a function of the thickness of gold membrane.

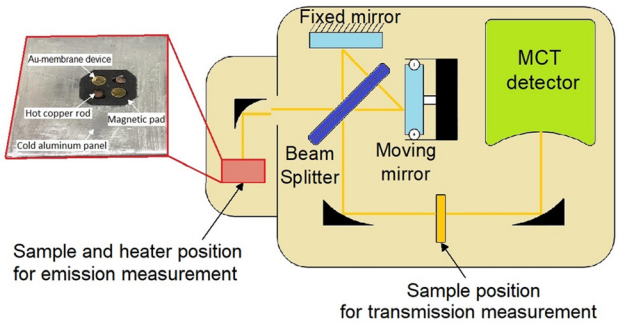


FIG. 3. Schematic diagram of the measurement setup. The FTIR spectrometer with a liquid nitrogen cooled mercury cadmium telluride (MCT) detector was used to measure the sample absorption and emission. The inset (left) shows the Au-membrane devices mounted on the heating fixture. The sample positions for the emission and transmission measurements are shown.

at $\lambda_r = \Lambda$, followed by the 2nd order (1,1) Wood's anomaly at $\lambda_r = \Lambda/\sqrt{2}$.[20,21] The diffracted waves are parallel to the surface at the Wood's anomalies resulting in vanishing transmission and maximum reflectance. At the resonance wavelength, the local electric fields are significantly enhanced as shown in Fig. S1 (supplementary material). A linear relation between the EOT peak and the device period is shown in Fig. 2(c). Moreover, the bandwidth of the resonance peak can be tuned by changing the gold thickness as demonstrated in Fig. 2(d). For membranes with $\Lambda = 2.5\,\mu$m and $\Lambda = 4.0\,\mu$m both coated with a 30 nm gold layer, full-width half-maximums (FWHMs) are 0.54 $\mu$m and 0.72 $\mu$m, respectively. The FWHM values reduce to 0.12 $\mu$m and 0.30 $\mu$m by increasing the gold layer thickness to 500 nm. The increase in the gold film thickness also causes a lower transmission coefficient and a higher absorptivity at the resonance wavelength. Tuning the Au-membrane period and thickness can generate a narrowband plasmonic resonance in the desired IR range, which makes the membrane device a promising selective IR emitter.

The optical response and mid-IR emission of the Au membrane devices were characterized using a Fourier transform infrared (FTIR) spectrometer (MB 155, ABB Bomem) as schematically shown in Fig. 3. A spectrum in the range of 2 $\mu$m to 6 $\mu$m was produced following a Fourier transform of the interferogram with a spectral resolution of 8 $\text{cm}^{-1}$. During the measurements, the device was perpendicular to the propagation direction of the mid-IR beam. The divergence angle of the IR beam was less than 1° and the beam covered the entire sample area including the Au-membrane and nickel grid. Transmission spectra of Au-membrane devices with the thicknesses of $t_{Au} = 50$ nm and $t_{Au} = 100$ nm and array periods of $\Lambda = 2.5\,\mu$m and $\Lambda = 4.0\,\mu$m were collected and normalized to the transmittances of a blank metal grid without any membrane. Figure 4(a) compares the measured EOT spectra of the membranes with $t_{Au} = 50$ and 100 nm. The membrane with $\Lambda = 2.5\,\mu$m and $t_{Au} = 50$ nm exhibits surface plasmon resonance at $\lambda_r = 2.90\,\mu$m with a full width at half maximum (FWHM) of 0.45 $\mu$m, and at the resonance, the transmission coefficient is as high as $T = 69.4\%$. The long period membrane ($\Lambda = 4.0\,\mu$m) demonstrates a resonant peak at $\lambda_r = 4.75\,\mu$m and FWHM = 0.9 $\mu$m, and the transmission coefficient is as high as $T = 76.8\%$. When the thickness of the membrane increases, the transmission coefficient at the resonant

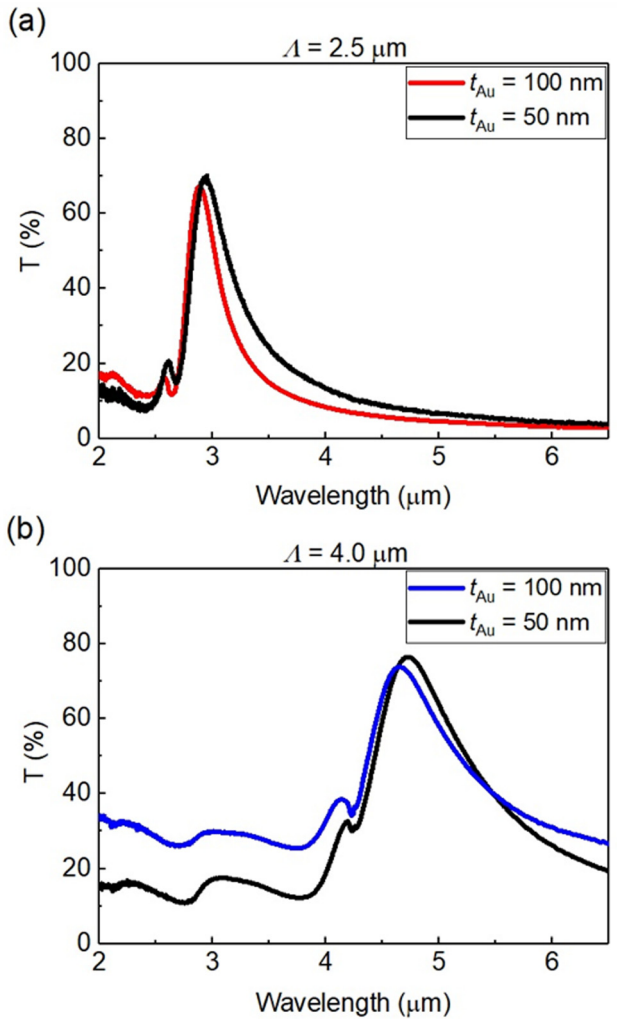


FIG. 4. Measured EOT spectra of the Au-membrane devices using the FTIR spectrometer. (a) EOT spectra of devices with $\Lambda = 2.5\,\mu$m and the gold thicknesses of $t_{Au} = 100$ nm (red) and 50 nm (black). (b) EOT spectra of devices with $\Lambda = 4.0\,\mu$m and the gold thicknesses of $t_{Au} = 100$ nm (blue) and 50 nm (black).

wavelength decreases, whereas the membrane becomes more absorbing. As shown in Fig. 4, when the membrane thickness increased to $t_{Au} = 100$ nm, the transmittance resonance bandwidth of the membranes reduced significantly. The transmission coefficients and FWHMs for the $\Lambda = 2.5\,\mu$m and $\Lambda = 4.0\,\mu$m devices are $T = 67.6\%$ and FWHM = 0.32 and $T = 73.9\%$ and FWHM = 0.8 $\mu$m, respectively.

According to the Kirchhoff's law of thermal radiation, the emissivity of the device, $\varepsilon(\lambda)$, is proportional to its absorbance $[\alpha(\lambda)]$. Here, our goal is to trim the mid-IR radiation spectrum by engineering the structure of the gold membrane. For a device of a thin plasmonic film fabricated on a substrate, the emissivity of the sample is given by $\varepsilon(\lambda) = \alpha(\lambda) + \varepsilon_{sub}(\lambda)T(\lambda)$, where $T(\lambda)$ is the transmittance of the sample and $\varepsilon_{sub}(\lambda)$ is the emissivity of the substrate material.[23] Depending on the transmission coefficient, the substrate material will interfere with the emission characteristics of the device. In contrast, for the free-standing membrane emitter, the substrate is eliminated, and the sample emission only relies on the absorption characteristics of the gold plasmonic membrane.

The near-IR and mid-IR radiation spectra of the Au-membranes were characterized in the wavelength range of

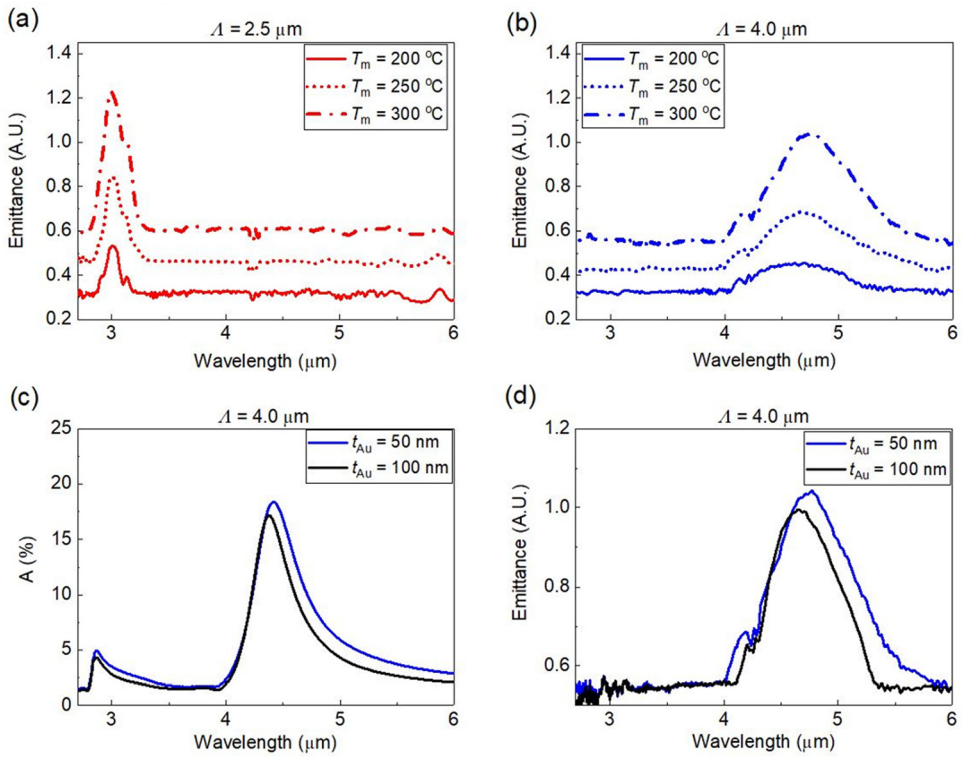


FIG. 5. Measured infrared emission spectra. (a) and (b) show the emission spectra measured at three different temperatures for the short-period sample ($\Lambda = 2.5\ \mu$m and $t_{Au} = 50$ nm) and long-period sample ($\Lambda = 2.5\ \mu$m and $t_{Au} = 50$ nm), respectively. (c) Simulated absorption spectra of the $\Lambda = 2.5\ \mu$m device with $t_{Au} = 50$ nm (blue) and 100 nm (black). (d) Measured infrared emission spectra ($T_m = 200\ ^\circ$C) of the devices with $t_{Au} = 50$ nm (blue) and 100 nm (black).

2 $\mu$m to 6 $\mu$m at elevated temperatures, using a heater that is designed to heat up small samples as shown in Fig. S2 (supplementary material). Figure 5(a) shows the emittance of the membrane with $\Lambda = 2.5\ \mu$m measured at $T_m = 200\ ^\circ$C, 250 °C, and 300 °C, respectively. Compared to the emission feature of a planar gold film (Fig. S3 in the supplementary material), the heated device exhibits a narrowband near-IR emission with the peak wavelength and FWHM of 3.0 $\mu$m and 0.5 $\mu$m, respectively. The emission spectra of the device with $\Lambda = 4.0\ \mu$m are shown in Fig. 5(b). The spectral positions of the thermal radiations are close to the EOT resonance shown in Figs. 4(a) and 4(b). The results manifest the fact that the emission is associated with the EOT resonance and can be tuned using the array period. In addition, for both devices, the emission intensity increases with the device temperature. The emission intensity increases by a factor of three when the device temperature raises from 200 to 300 °C.

We also investigated the effect of the membrane thickness on the emittance. The simulation results in Fig. 2(d) suggest that the bandwidth of thermal emission can be narrowed down by increasing the thickness of the gold film. Using the Au-membrane device with the period of 4.0 $\mu$m as an example, the plasmonic membranes with thicknesses of $t_{Au} = 100$ nm and 50 nm were studied using simulation and experiment. The simulation results in Fig. 5(c) compare the absorption spectra of the devices, and the FWHMs for the 100-nm-thick and 50-nm-thick membranes are 0.4 $\mu$m and 0.48 $\mu$m, respectively. As shown in Fig. 5(d), the bandwidth of the thermal emission decreases from 0.82 $\mu$m to 0.69 $\mu$m, when the membrane thickness increases from 50 nm to 100 nm. By doubling the value of $t_{Au}$, the FWHM decreases 16% and the emission spectrum shows a blue shift, which is approximately 1.7% of peak emission wavelength.

In conclusion, we studied the thermal emission of the free-standing gold membranes with a 2D subwavelength array of holes. The Au-membrane devices with grating periods of 2.5 $\mu$m and 4 $\mu$m were fabricated and characterized for their optical transmission and thermal emission. The EOT of the Au-membrane devices showed the transmission coefficient as high as 76.8% and an absorption coefficient of 23.1%. When heated above room temperature, the membrane devices exhibit narrowband emission in the near-IR and mid-IR wavelength ranges from 2.5 $\mu$m to 5.5 $\mu$m. The emission wavelength and bandwidth can be effectively tuned using the grating period and membrane thickness, respectively.

The free-standing plasmonic device offers several beneficial features: (i) The use of a free-standing membrane without a substrate eliminates the effect of substrate thermal emission and multiple SPR modes. The thermal emission can be fully determined using the single SPR modes of the Au membrane. (ii) The emission characteristics, including spectral range and bandwidth, can be precisely tuned by trimming the structure of the device. (iii) Without heat dissipations through a substrate, a high emission conversion could be achieved. (iv) Compared to substrate based emitters, the thin membrane has low heat capacity and rapid response times. These attributes are desirable for sensor applications. On the other hand, the membrane device is relatively fragile and needs to be heated uniformly to prevent damages. In future, the Au-membrane emitter can be improved by the application of electric resistance heating to raise device temperature by the following current through

the membrane. In addition, we will apply a vacuum seal to isolate the membrane from the atmosphere and thus eliminate the heat dissipation through the air convection. The development of selective IR emitters with a simple structure, inexpensive fabrication approach, and widely tunable spectral signature will benefit a broad range of fields. We envision that the membrane-based device can be used in chemical analysis, biomolecule sensing, and thermal imaging as a lightweight, portable, low cost, and narrowband infrared light source.

See supplementary material for the simulated nearfield distributions for the resonant modes, the customized apparatus that can heat up the devices, and the emission spectrum of a planar gold film at 300 °C.

This work was supported by the National Science Foundation Grant No. ECCS 16-53673, NSF Grant No. CMMI CMMI-1265844, the Exploratory Research Program of Iowa State University, and the 3M Non-Tenured Faculty Award. The content is solely the responsibility of the authors and does not necessarily represent the official views of the National Science Foundation and 3M.

[1]H. A. Atwater and A. Polman, Nat. Mater. **9**(3), 205–213 (2010).
[2]J. N. Anker, W. P. Hall, O. Lyandres, N. C. Shah, J. Zhao, and R. P. Van Duyne, Nat. Mater. **7**(6), 442–453 (2008).
[3]F. Wang and Y. R. Shen, Phys. Rev. Lett. **97**(20), 206806 (2006).
[4]B. Temelkuran, M. Bayindir, E. Ozbay, R. Biswas, M. M. Sigalas, G. Tuttle, and K. M. Ho, J. Appl. Phys. **87**(1), 603–605 (2000).
[5]J. F. Zhu, M. Xue, H. J. Shen, Z. Wu, S. Kim, J. J. Ho, A. Hassani-Afshar, B. Q. Zeng, and K. L. Wang, Appl. Phys. Lett. **98**(15), 151110 (2011).
[6]Y. F. Zhao, L. J. Liu, X. W. Zhao, and M. Lu, Appl. Phys. Lett. **109**(7), 071108 (2016).
[7]Y. F. Zhao, M. F. Cao, J. F. McClelland, Z. Y. Shao, and M. Lu, Biosens. Bioelectron. **85**, 261–266 (2016).
[8]Z. W. Liu, W. B. Hou, P. Pavaskar, M. Aykol, and S. B. Cronin, Nano Lett. **11**(3), 1111–1116 (2011).
[9]X. H. Huang, P. K. Jain, I. H. El-Sayed, and M. A. El-Sayed, Laser Med. Sci. **23**(3), 217–228 (2008).
[10]K. Ikeda, H. T. Miyazaki, T. Kasaya, K. Yamamoto, Y. Inoue, K. Fujimura, T. Kanakugi, M. Okada, K. Hatade, and S. Kitagawa, Appl. Phys. Lett. **92**(2), 021117 (2008).
[11]M. De Zoysa, T. Asano, K. Mochizuki, A. Oskooi, T. Inoue, and S. Noda, Nat. Photonics **6**(8), 535–539 (2012).
[12]T. Inoue, M. De Zoysa, T. Asano, and S. Noda, Appl. Phys. Express **7**(1), 012103 (2014).
[13]M. U. Pralle, N. Moelders, M. P. McNeal, I. Puscasu, A. C. Greenwald, J. T. Daly, E. A. Johnson, T. George, D. S. Choi, I. El-Kady, and R. Biswas, Appl. Phys. Lett. **81**(25), 4685–4687 (2002).
[14]F. Kusunoki, J. Takahara, and T. Kobayashi, Electron. Lett. **39**(1), 23–24 (2003).
[15]J. G. Fleming, S. Y. Lin, I. El-Kady, R. Biswas, and K. M. Ho, Nature **417**(6884), 52–55 (2002).
[16]S. Enoch, J. J. Simon, L. Escoubas, Z. Elalmy, F. Lemarquis, P. Torchio, and G. Albrand, Appl. Phys. Lett. **86**(26), 261101 (2005).
[17]D. L. C. Chan, M. Soljacic, and J. D. Joannopoulos, Phys. Rev. E **74**(1), 016609 (2006).
[18]S. Y. Lin, J. Moreno, and J. G. Fleming, Appl. Phys. Lett. **83**(2), 380–382 (2003).
[19]M. W. Tsai, T. H. Chuang, C. Y. Meng, Y. T. Chang, and S. C. Lee, Appl. Phys. Lett. **89**(17), 173116 (2006).
[20]A. Peer and R. Biswas, Nanoscale **8**(8), 4657–4666 (2016).
[21]R. Biswas, S. Neginhal, C. G. Ding, I. Puscasu, and E. Johnson, J. Opt. Soc. Am. B **24**(10), 2589–2596 (2007).
[22]L. J. Liu, H.-Y. Wu, and M. Lu, in *CLEO: Science and Innovations* (Optical Society of America, San Jose, 2017), pp. SM3N-2.
[23]G. Fabbri, P. Baraldi, and P. Frassoldati, Ann. Chim. **65**(5–6), 301–304 (1975).
[24]S. Babar and J. H. Weaver, Appl. Opt. **54**(3), 477–481 (2015).